AMERICAN SOCIETY FOR MICROBIOLOGY | Antimicrobial Agents and Chemotherapy®

EXPERIMENTAL THERAPEUTICS

# A Fluorinated Phenylbenzothiazole Arrests the *Trypanosoma cruzi* Cell Cycle and Diminishes the Infection of Mammalian Host Cells

**Roberto I. Cuevas-Hernández,[a,b] Richard M. B. M. Girard,[b] Sarai Martínez-Cerón,[a] Marcelo Santos da Silva,[c,d] Maria Carolina Elias,[c,d] Marcell Crispim,[b] José G. Trujillo-Ferrara,[a] Ariel Mariano Silber[b]**

[a]Laboratory of Biochemistry Research, Escuela Superior de Medicina, Instituto Politécnico Nacional, México Plan de San Luis Y Díaz Mirón S/N, Casco de Santo Tomas, Miguel Hidalgo, Mexico City, Mexico

[b]Laboratory of Biochemistry of Tryps–LaBTryps, Department of Parasitology, Institute of Biomedical Sciences, University of São Paulo, Cidade Universitária, São Paulo, Brazil

[c]Special Laboratory of Cell Cycle, Butantan Institute, São Paulo, Brazil

[d]Centre of Toxins, Immune Response and Cell Signalling–CeTICS, Butantan Institute, São Paulo, Brazil

**ABSTRACT** Chagas disease (CD) is a human infection caused by *Trypanosoma cruzi*. CD was traditionally endemic to the Americas; however, due to migration it has spread to countries where it is not endemic. The current chemotherapy to treat CD induces several side effects, and its effectiveness in the chronic phase of the disease is controversial. In this contribution, substituted phenylbenzothiazole derivatives were synthesized and biologically evaluated as trypanocidal agents against *Trypanosoma cruzi*. The trypanocidal activities of the most promising compounds were determined through systematic *in vitro* screening, and their modes of action were determined as well. The physicochemical-structural characteristics responsible for the trypanocidal effects were identified, and their possible therapeutic application in Chagas disease is discussed. Our results show that the fluorinated compound 2-methoxy-4-[5-(trifluoromethyl)-1,3-benzothiazol-2-yl] phenol (BT10) has the ability to inhibit the proliferation of epimastigotes [$IC_{50(Epi)} = 23.1 \pm 1.75\ \mu M$] and intracellular forms of trypomastigotes [$IC_{50(Tryp)} = 8.5 \pm 2.9\ \mu M$] and diminishes the infection index by more than 80%. In addition, BT10 has the ability to selectively fragment 68% of the kinetoplastid DNA compared with 5% of nucleus DNA. The mode of action for BT10 on *T. cruzi* suggests that the development of fluorinated phenylbenzothiazole with electron-withdrawing substituent is a promising strategy for the design of trypanocidal drugs.

**KEYWORDS** phenylbenzothiazole, chemotherapy, *Trypanosoma cruzi*, kDNA, antiparasitic agents

American trypanosomiasis, or Chagas disease (CD), is a zoonosis caused by the flagellated intracellular protist *Trypanosoma cruzi*. According to the World Health Organization (WHO), CD is endemic to the Americas; however, due to migration, it has spread to countries where it is not endemic, such as Canada and several European and Western Pacific countries (1, 2). This disease, with approximately 7 million affected people, causes approximately 14 thousand deaths annually, and there are 70 million at risk of becoming infected (3). *T. cruzi*, which is naturally transmitted by hematophagous insects of the *Reduviidae* family, can also be transmitted by other routes, such as congenitally (from an infected pregnant woman to the fetus), orally (through contaminated foods and liquids), and through organ transplantations and blood transfusions (4).

*T. cruzi* has a complex life cycle within invertebrate and vertebrate hosts (5–7).

**Citation** Cuevas-Hernández RI, Girard RMBM, Martínez-Cerón S, Santos da Silva M, Elias MC, Crispim M, Trujillo-Ferrara JG, Silber AM. 2020. A fluorinated phenylbenzothiazole arrests the *Trypanosoma cruzi* cell cycle and diminishes the infection of mammalian host cells. Antimicrob Agents Chemother 64:e01742-19. https://doi.org/10.1128/AAC.01742-19.



Address correspondence to José G. Trujillo-Ferrara, jtrujillo@ipn.mx, or Ariel Mariano Silber, asilber@usp.br.

**Received** 27 August 2019
**Returned for modification** 29 September 2019
**Accepted** 1 November 2019
**Accepted manuscript posted online** 11 November 2019
**Published** 27 January 2020

Replicative, noninfective epimastigotes present in the insect vector give rise to nonreplicative infective metacyclic trypomastigotes. These forms invade the host cell, establish the infection, and differentiate into replicative amastigotes. Amastigote forms give rise to a transient stage, named intracellular epimastigotes, which subsequently differentiate into trypomastigotes that can disseminate in the mammalian host through the bloodstream after causing lysis of host cells and are capable of infecting other cells. The insect vector can acquire these forms during its bloodmeal, becoming infected and able to infect a new mammalian host (8, 9).

Human infection is characterized by two sequential clinical phases: acute and chronic. The acute phase is often asymptomatic and usually remains undiagnosed. Most infected individuals proceed to the chronic phase, which lasts for the rest of the patient's life. The chronic phase presents several clinical forms: 70% of patients are asymptomatic, while the remaining 30% present clinical manifestations, with the most frequent being chagasic chronic cardiomyopathy and, more rarely, megavisceras (mainly megacolon and megaesophagus). Over years, the cardiac form of the infection can cause sudden death or heart failure due to the progressive destruction of the cardiac muscle (9).

A century after the discovery of the disease by Carlos Chagas in 1909, only two nitroheterocyclic drugs, nifurtimox and benznidazole, are used to treat *T. cruzi* infection. These drugs are effective during acute infection. However, their effectiveness during the chronic phase of CD is controversial due to their toxicity (10). Therefore, more secure, effective, and accessible alternatives are currently being sought to treat CD.

*T. cruzi*, along with other trypanosomatids, possesses unique morphological and metabolic features, offering opportunities for looking for selective inhibitors. Among them, it is worth mentioning the kinetoplast, a complex structure bearing the mitochondrial genome referred to as kinetoplast DNA or kDNA. The kDNA consists of a large number of relaxed circular DNA molecules interlocked with each other to form a catenated DNA network, and this feature is among those that have frequently been considered promising therapeutic targets because they are exclusive to trypanosomatids (11).

In the last 2 decades, large libraries of compounds of diverse chemical nature have been screened for trypanocidal agents (12). Among the selected chemical structures, benzothiazoles (BZTs) have been studied in detail and have been suggested as trypanocides (13–15). BZTs are a class of bicyclic compounds with a broad spectrum of biological applications, such as neuroprotectors (16), anticonvulsants (17), antioxidants (18), kinase inhibitors (19), anticancer agents (20, 21), antimicrobials (22), and leishmanicidals (23). In particular, it has been suggested that the trypanocidal effects of benzothiazoles are related to the inhibition of triosephosphate isomerase (TIM) (24, 25). In previous work, we reported the development of 4-[5-(trifluoromethyl)-1,3-benzothiazol-2-yl] benzoic acid, named BT3, which showed excellent trypanocidal activity on bloodstream trypomastigotes of *T. cruzi* (14); thus, it was proposed as a new nucleus for the development of trypanocidal agents. The aim of this contribution was to determine the trypanocidal activity of a collection of 14 benzothiazoles structurally related to BT3. We evaluated their anti-*T. cruzi* activity and analyze their physicochemical-structural characteristics responsible for its biological activity. BT10, the most promising molecule due to its higher selectivity index than the other derivatives, was selected for further analyzing its effects on different aspects of *T. cruzi* biology. We propose BT10 as a promising pharmacological hit compound for developing a treatment against CD.

## RESULTS

**BT10 affects the proliferation of *T. cruzi* epimastigotes.** A collection of 14 structurally related molecules, named BT1 to BT14, was synthesized (Fig. 1A). The identification of the synthesized molecules and their chemical characterization were performed by melting point (mp), nuclear magnetic resonance (NMR), and electrospray ionization-mass spectrometry spectra determination (ESI-MS). These compounds were

**A**

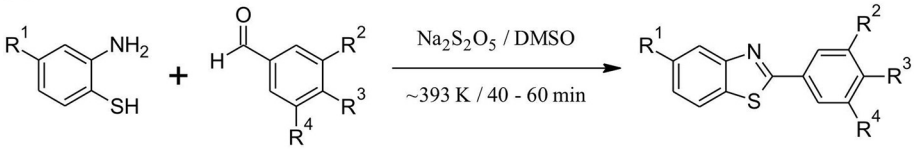


2 - Phenylbenzothiazole derivatives

| | $R^1$ |
|---|---|
| A | H |
| B | $CF_3$ |

| | $R^2$ | $R^3$ | $R^4$ |
|---|---|---|---|
| C | H | H | H |
| D | H | COOH | H |
| E | H | $COOCH_3$ | H |
| F | $OCH_3$ | OH | H |
| G | COOH | H | H |
| H | $COOCH_3$ | H | H |
| I | $OCH_3$ | OH | $OCH_3$ |
| J | H | CN | H |
| K | H | Cl | H |
| L | H | Br | H |

**(BT1-14)**

| ID | $R^1$ | $R^2$ | $R^3$ | $R^4$ |
|---|---|---|---|---|
| **BT1** | H | H | H | H |
| **BT2** | H | H | COOH | H |
| **BT3** | $CF_3$ | H | COOH | H |
| **BT4** | $CF_3$ | H | H | H |
| **BT5** | $CF_3$ | H | $COOCH_3$ | H |
| **BT6** | H | $OCH_3$ | OH | H |
| **BT7** | H | COOH | H | H |
| **BT8** | H | H | $COOCH_3$ | H |
| **BT9** | H | $COOCH_3$ | H | H |
| **BT10** | $CF_3$ | $OCH_3$ | OH | H |
| **BT11** | H | $OCH_3$ | OH | $OCH_3$ |
| **BT12** | H | H | CN | H |
| **BT13** | H | H | Cl | H |
| **BT14** | H | H | Br | H |

**B**

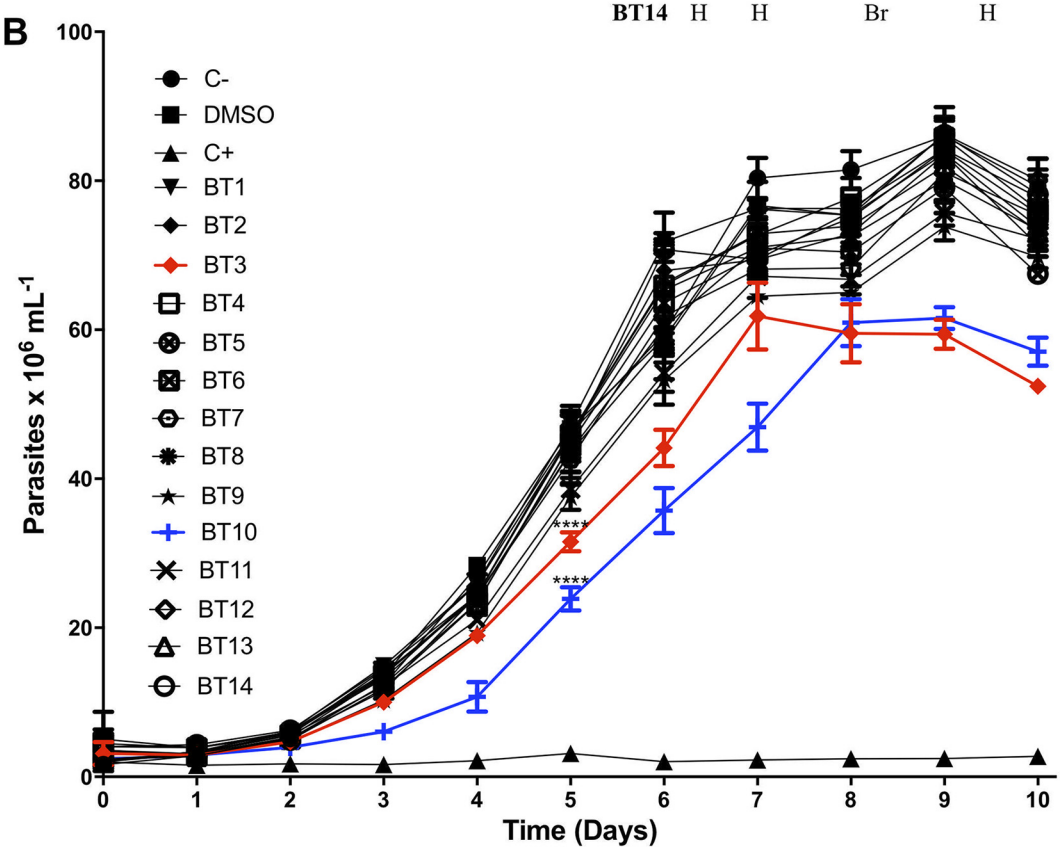


**FIG 1** Synthesis of 2-phenylbenzothiazole derivatives and screening assay for selection of the best active compounds on the proliferation growth curves of epimastigote forms of *T. cruzi*. (A) Schematic synthesis strategy and structure of 2-phenylbenzothiazole derivatives. (B) Growth curves in the presence of 25 $\mu$M each compound proposed. A combination of 60 $\mu$M rotenone with 0.5 $\mu$M antimycin was used as a positive control (C+). The figure shows a representative proliferation curve from three independent experiments. The values are plotted as the means ± standard deviations (SD) and compared on the 5th day of proliferation to the control (C−) using a *t* test. ****, $P < 0.0001$ to establish significant differences.

initially evaluated for their ability to inhibit epimastigote proliferation in the presence of 25 $\mu$M BT1-14. We attributed a positive inhibition activity to those compounds that, at the concentration used, were able to diminish the cell density at the mid-exponential growth phase (which was measured on the 5th day from the beginning of incubation) by 50% or more. Epimastigotes cultured in the absence of drugs in the presence or absence of DMSO (which did not show significant differences) were used as negative controls for inhibition, and their cell density was considered 100% proliferation. For a positive control for the inhibition of cell proliferation, the parasites were incubated in the presence of a combination of 60 $\mu$M rotenone plus 0.5 $\mu$M antimycin (RA). The compound BT10 was identified as having trypanocidal or trypanostatic activity. BT10 produced a diminution of cell density of 50% compared to that of control (untreated) cultures. Despite not reaching the criterion for selecting them as trypanocidal/trypanostatic, it is worth mentioning that compounds BT3, BT9, and BT11 showed a modest but statistically significant decrease in cell density concentration compared to that of controls (Fig. 1B; see also Fig. S1 in the supplemental material). Because BT3 was used as the lead (14) for choosing and synthesizing BT1 to BT14, it was selected for further experiments so as to use this information to unveil the structure/activity relationship of these compounds.

To further evaluate the potency of BT3 and BT10 as anti-*T. cruzi* agents, we initially determined their 50% inhibitory concentrations ($IC_{50}$) on epimastigote proliferation through dose-response experiments. Cells were cultured in liver infusion tryptose (LIT) in the presence of different concentrations of BT3 and BT10. As previously described, epimastigotes cultured in the absence of drugs were used as negative controls for inhibition, and their cell density was considered 100% proliferation; parasites treated with RA were used as positive controls for the inhibition of cell proliferation. As expected, BT3 and BT10 showed a dose-dependent inhibition of epimastigote proliferation, with $IC_{50}$ values of 48.8 $\pm$ 5.77 $\mu$M and 23.1 $\pm$ 1.75 $\mu$M, respectively (Fig. 2A and B).

**BT10 does not induce PCD.** To characterize the mechanism of action of BT10, we initially investigated its ability to trigger programmed cell death (PCD) in *T. cruzi* epimastigotes. For this analysis, we investigated the typical PCD morphological, cellular, and biochemical hallmarks in trypanosomatids, such as reactive oxygen species (ROS) production, as well as $Ca^{2+}$ and mitochondrial inner membrane potential ($\Delta\Psi_m$) imbalance (26, 27). We initially looked for exposure of phosphatidylserine in the external leaflet of the plasma membrane. Parasites were treated with 25 $\mu$M and 50 $\mu$M BT10 (approximately 1$\times$ and 2$\times$ the $IC_{50}$). After washing, they were incubated with annexin V-fluorescein isothiocyanate (FITC) to assess external exposure of phosphatidylserine and propidium iodide (PI) to assess plasma membrane permeabilization. The cells were then subjected to analysis by flow cytometry. The results showed that BT10 did not induce alterations in the plasma membrane; no exposure of phosphatidylserine or signs of membrane permeabilization were evidenced at the two concentrations used in the assay compared with that of the controls (Fig. 3A to C). We also investigated whether BT10 triggered other PCD hallmarks, such as the dissipation of the mitochondrial inner membrane potential ($\Delta\Psi_m$), production of ROS, and changes in the cytosolic $Ca^{2+}$ levels (28). To analyze membrane depolarization ($\Delta\Psi_m$), parasites treated with 25 or 50 $\mu$M BT10 (or left untreated as a control) for 5 days were stained with rhodamine 123 (Rh123) for 20 min at 28°C and further analyzed by flow cytometry. Treated parasites showed a shift in the obtained fluorescence values, showing an alteration of $\Delta\Psi_m$ (Fig. 3D). To determine the possible variations of the intracellular $Ca^{2+}$ concentrations, epimastigotes were incubated with 25 $\mu$M BT10 (or left untreated as a control) for 5 days. After treatment, the parasites were incubated with Fluo-4 and analyzed by flow cytometry. The results showed that treated parasites exhibited increased intracellular $Ca^{2+}$ concentrations compared with those of untreated parasites (control) (Fig. 3E). Finally, to evaluate possible changes in the production of $H_2O_2$ due to treatment with BT10, epimastigotes treated with 25 $\mu$M BT10 for 24 h (or left untreated

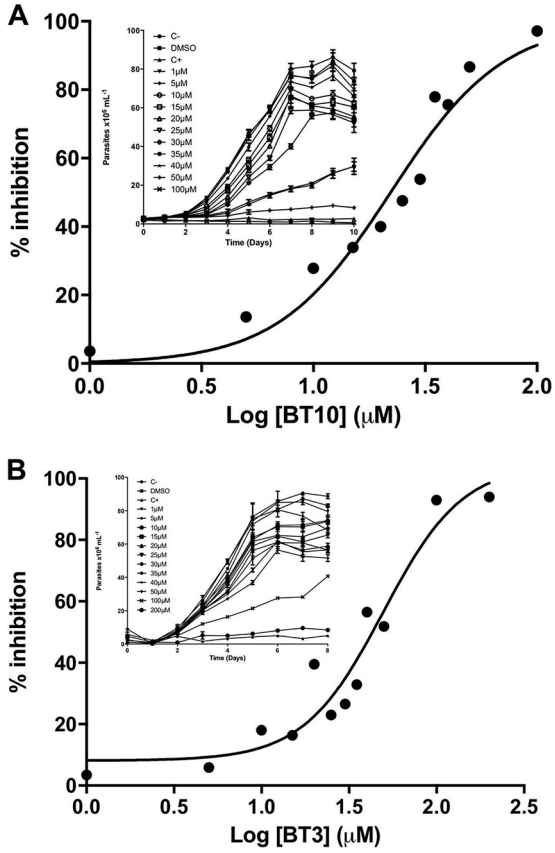


**FIG 2** Effects of BT3 and BT10 on the proliferation of the epimastigote form of *Trypanosoma cruzi*. (A) Growth inhibition curves in the presence of different concentrations of BT10 at 28°C, which is the optimum temperature of proliferation ($IC_{50}$ = 23.1 ± 1.75 μM). (B) Growth inhibition curves in the presence of different concentrations of BT3 at 28°C ($IC_{50}$ = 48.8 ± 5.77 μM). A combination of 60 μM rotenone with 0.5 μM antimycin was used as a positive control (C+). The $IC_{50}$ values were obtained by adjusting the data to nonlinear regression. Panels show representative proliferation curves from three independent experiments for each condition.

as a control) were labeled with 6-carboxy-2′,7′-dichlorodihydrofluorescein diacetate (carboxy-DCFDA). The results showed that the treated parasites did not produce a greater amount of $H_2O_2$ than untreated parasites (Fig. 3F). Taken together, these results indicate that BT10 does not trigger any of the types of classic cell death as a primary effect, even at high concentrations. However, mitochondrial inner membrane depolarization and alterations in $Ca^{2+}$ concentrations could be critical factors affecting the proliferation or long-term survival of parasites.

As the previous results suggest that BT10 did not trigger cell death, we hypothesized that the drug interferes with the *T. cruzi* cell cycle. To confirm this possibility, we evaluated the reversibility of the effect of BT10 on epimastigote proliferation. Epimastigotes were left untreated (control) or treated with 25 μM and 100 μM BT10. The treated parasites showed diminished proliferation during the treatment with respect to that of the controls. This alteration was reversed by washing out BT10, indicating that BT10 reversibly inhibited epimastigote proliferation (Fig. S2). On this basis, we further analyzed possible alterations in the cell cycle. Parasites treated with 25 μM and 100 μM BT10 or left untreated (control) for 5 days were labeled with propidium iodide and submitted to cell cycle analysis by flow cytometry (Fig. 4A). The data collected showed a significant decrease in cells in the $G_0/G_1$ phases and an accumulation in the $G_2$/M phase, with significant alterations in the S phase at 100 μM BT10 compared to those in the control cells (Fig. 4B).

Importantly, an accumulation of cells in the $G_2$/M phases is usually due to an arrest of the cell cycle at the $G_2$ checkpoint, in which DNA integrity is sensed and checked

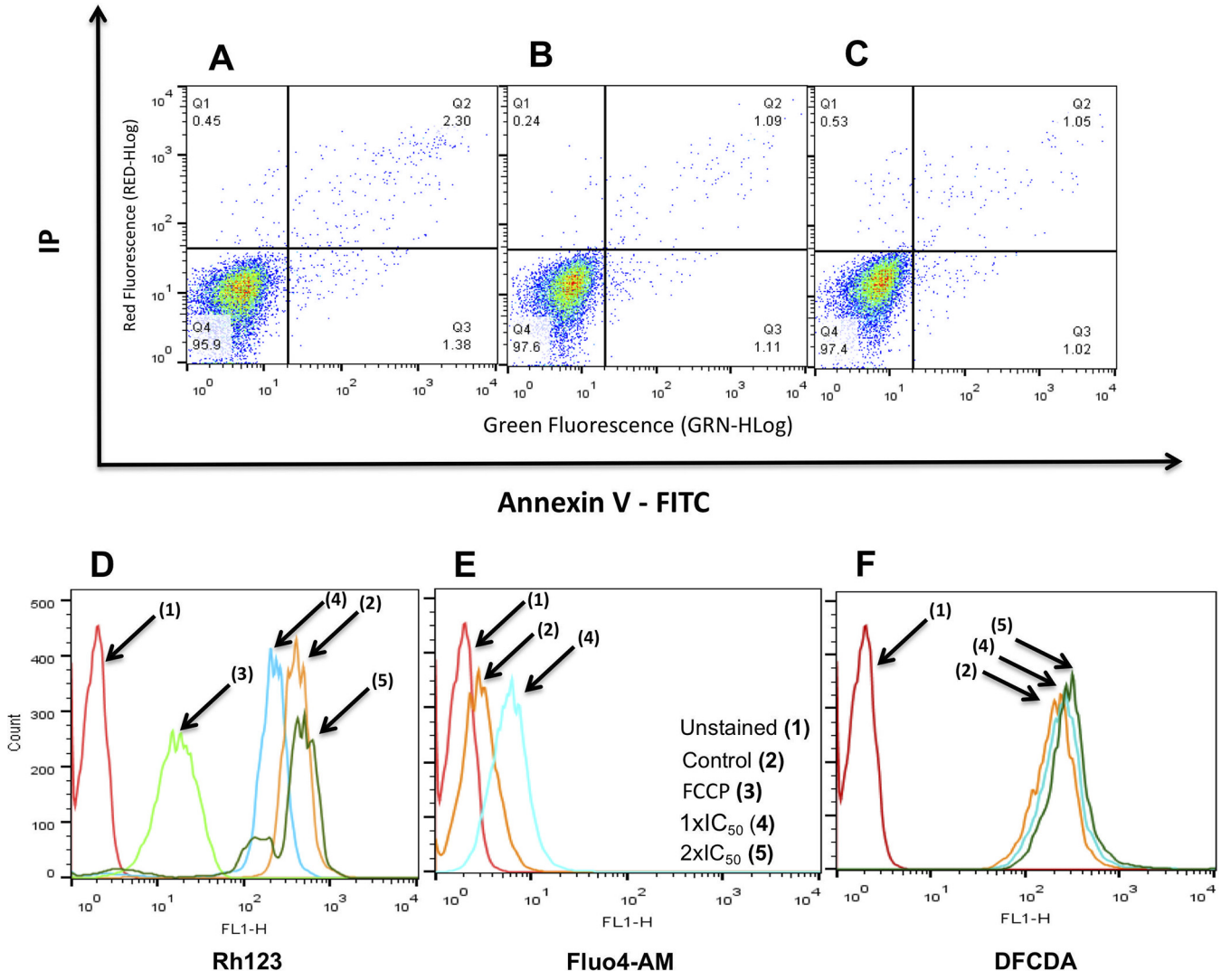


**FIG 3** Analysis of cell death type and viability in epimastigotes treated with BT10. (A to C) Analysis of extracellular exposure of phosphatidylserine by annexin V/propidium iodide labeling by flow cytometry on epimastigotes treated with BT10 for 5 days: nontreated parasites (A), parasites treated with 1× $IC_{50}$ (25 $\mu$M) BT10 (B), and parasites treated with 2× $IC_{50}$ (50 $\mu$M) BT10 (C). IP, immunoprecipitation. (D to F) Analysis of cell viability of epimastigotes treated with BT10 for 5 days: membrane depolarization test ($\Delta\Psi_m$) (D), quantification of intracellular $Ca^{2+}$ (E), and analysis of the generation of ROS after 24 h of treatment with BT10 (F). Panels are representative of three independent experiments. The values were plotted as the means ± standard errors of the means (SEM) and compared to the control using a *t* test. *, $P < 0.05$ to establish significant differences.

(29). Because cell cycle arrest can be induced at the $G_2$ checkpoint by DNA damage (30, 31), we investigated whether BT10 causes DNA damage to treated parasites. We analyzed the effect of BT10 on both genomic DNA (gDNA) and kDNA integrity using a terminal deoxynucleotidyltransferase-mediated dUTP-biotin nick end labeling (TUNEL) assay. Epimastigotes treated for 5 days with 25 $\mu$M BT10 (or left untreated as a control) were submitted to the TUNEL assay. The parasites were initially analyzed by flow cytometry, showing differences in fluorescence intensity in the treated population with respect to that of the control (Fig. 5B). When the parasites were analyzed by microscopy, we found that the kDNA was intensively labeled compared to the gDNA in the parasites treated with BT10. Untreated parasites and treated parasites exhibited 35.2% ± 6.2% and 67.6% ± 8.6%, respectively, of cells with labeled kDNA. On the other hand, the percentage of treated parasites with labeled gDNA was 5.4% ± 1.2%, while the untreated parasites remain unlabeled. These data indicate that BT10 selectively triggers kDNA damage (Fig. 5A). Taken together, these data indicate that BT10 induces DNA double-strand breaks preferentially on kDNA.

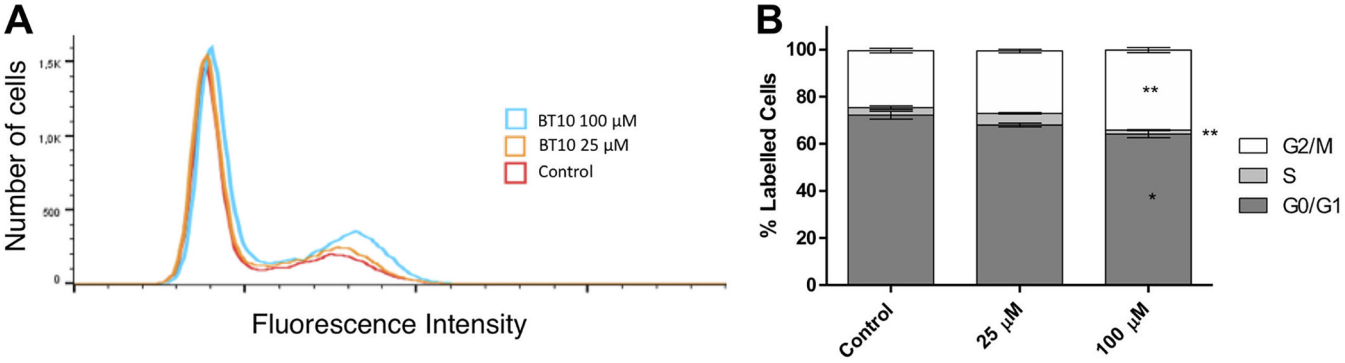


**FIG 4** Effect of BT10 on the epimastigote cell cycle using fluorescence-activated cell sorting (FACS). Cells were left untreated (control) or were treated with 25 $\mu$M or 100 $\mu$M BT10 for 5 days during exponential growth. After that time, parasites were washed, treated with RNase A, and stained with propidium iodide, and their DNA content was analyzed by FACS. In total, 50,000 events were analyzed for each sample. Histograms are shown in panel A, and quantification of the percentage of cells labeled in each stage of the cell cycle is presented in panel B. The figure shows representative histograms from three independent experiments. The values are plotted as the means $\pm$ SEM and compared to the control using a *t* test. *, $P < 0.05$; **, $P < 0.01$ (to establish significant differences). The data correspond to three independent biological experiments.

**Cytotoxicity of BT3 and BT10 to mammalian cells.** To further evaluate the effect of BT10 on the stages corresponding to mammalian host cell infection, it is necessary first to determine the range in which the compounds are nontoxic for the host cells. Therefore, CHO-$K_1$ cells were incubated in the presence of different concentrations of BT3 (ranging from 16 to 800 $\mu$M) or BT10 (ranging from 8 to 288 $\mu$M), and cytotoxicity was evaluated by MTT assay after 48 h of treatment. The concentrations corresponding to a measurement of 50% cytotoxicity ($CC_{50}$) were obtained from the typical sigmoidal concentration-response curves, resulting in 95.3 $\pm$ 3.3 $\mu$M for BT10 and 127.6 $\pm$ 0.9 $\mu$M for BT3 (Fig. 6A and B).

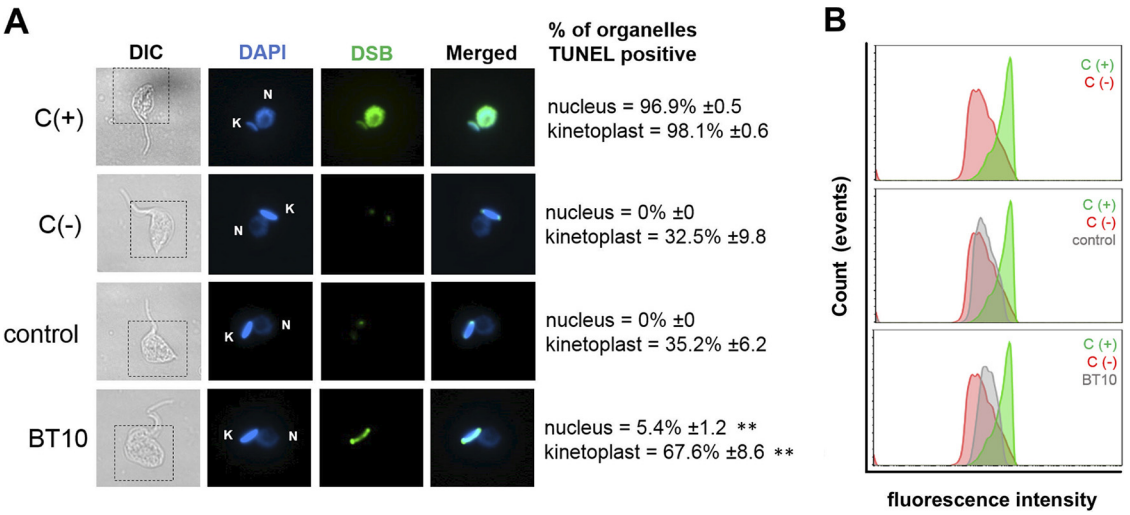


**FIG 5** BT10 induces increased kDNA fragmentation. (A) Control cells and cells treated with 25 $\mu$M BT10 for 5 days were submitted to TUNEL assay to indicate DNA strand breaks (DSBs; green). DAPI (blue) was used to show organelles that contain DNA (N, nucleus; k, kinetoplast). Differential interference contrast (DIC) and merged columns indicate the morphology of the cells and overlay between the DAPI and DSB columns, respectively. DNase I was used as a positive control, and the absence of TdT enzyme was used as a negative control. The percentage of TUNEL-positive organelles is displayed on the right of the panel. Images represent the pattern prevalent in each analysis. (B) The same groups were analyzed through flow cytometry, and the histograms (counts $\times$ fluorescence intensity $-$ BL1 area) were plotted to show differences in fluorescence intensity between each group (treated and nontreated) and controls (positive and negative). In total, 10,000 events were analyzed for each sample. The histograms shown are representative of three independent experiments. The increase in fluorescence intensity shown in the flow cytometry graphs and the percentage of TUNEL-positive organelles indicates that the BT10 compound is highly effective at generating an increased amount of DSBs within a single cell and in a larger number of cells. The values are plotted as the means $\pm$ SEM and compared to the control using a *t* test. **, $P < 0.01$ to establish significant differences. The data correspond to three independent biological experiments.

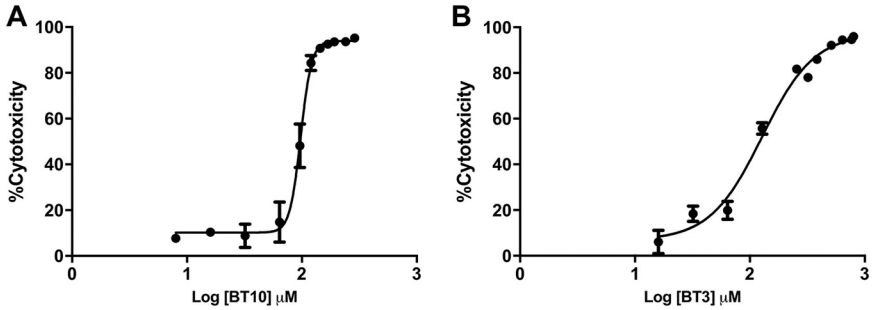


**FIG 6** Effect of BT10 and BT3 on mammalian cells. The cell viability of CHO-$K_1$ cells treated with different concentrations of BT10 or BT3 for 48 h was assessed by MTT assay, and the corresponding concentration-response curve of cytotoxicity was expressed as percent inhibition of proliferation. (A) Dose-response for cell viability in the presence of different concentrations of BT10 (range, 8 to 288 $\mu$M; $CC_{50}$ = 95.3 ± 3.3 $\mu$M). (B) Dose-response for cell viability in the presence of different concentrations of BT3 (range, 16 to 800 $\mu$M; $CC_{50}$ = 127.6 ± 0.9 $\mu$M). Panels show a representative curve from three independent experiments.

**BT10 selectively inhibits the intracellular cycle of *T. cruzi*.** According to the results obtained from the cytotoxicity experiments, a range of BT10 concentrations from 0.1 to 32 $\mu$M was selected to evaluate the $IC_{50}$ for trypomastigote release after an entire infection cycle on CHO-$K_1$ cells. To measure the effect of BT10 on trypomastigote production by infected host cells, CHO-$K_1$ cells were incubated with trypomastigotes for 4 h. The cells were washed to eliminate the noninternalized parasites and then incubated (or not; control) with culture medium at different concentrations of BT10. On the 5th day postinfection, the trypomastigotes released into the culture media were counted. We observed a dose-dependent decrease in trypomastigote release, which allowed us to measure the $IC_{50}$ for trypomastigote bursting [$IC_{50(Tryp)}$; 8.5 ± 2.9 $\mu$M) (Fig. 7A and B). Based on this value and the $CC_{50}$ obtained for the cytotoxicity of BT10 on CHO-$K_1$ cells, we obtained a selectivity index [SI; $CC_{50}/IC_{50(Tryp)}$] of 11.21. It is expected that the diminished number of burst trypomastigotes in the BT10-treated cells is a reflection of the diminished proliferation of intracellular forms. To verify this hypothesis, CHO-$K_1$ cells were incubated with trypomastigotes for 4 h. The cells were washed to eliminate the noninternalized parasites, and then they were incubated with culture medium supplemented (or not; control) with 8.5 $\mu$M BT10 (the concentration corresponding to the $IC_{50}$ obtained for trypomastigote bursting). On the second day postinfection, the cultures were fixed and stained, and the nuclei corresponding to the total number of cells, the number of infected cells, and the number of amastigotes per infected cell were counted. The percentage of infected cells and the number of intracellular amastigotes per cell were 8.6% ± 0.88% and 0.16 ± 0.05 for infected cells treated with 8.5 $\mu$M BT10 and 13.1% ± 3.7% and 0.6 ± 0.13 for untreated conditions (Fig. 7C and D). BT10 treatment diminished the number of infected cells by 33.8% and the average number of intracellular amastigotes per cell by 70.3%. The resulting infection index was 1.4 ± 0.48 for the treated infected cells and 8.9 ± 1.34 for the controls, indicating that the treatment reduced the infection index by 81.3% ± 6.94% (Fig. 7E and F). Taken together, these results indicate that treatment with 8.5 $\mu$M BT10 interferes with proliferation and/or differentiation of intracellular stages (Fig. 7).

## DISCUSSION

In the present work, we obtained and evaluated a collection of 14 benzothiazoles (BT1 to BT14) related to previously studied 4-[5-(trifluoromethyl)-1,3-benzothiazol-2-yl] benzoic acid (BT3), which showed relevant anti-*T. cruzi* trypomastigote activity (14). The antiproliferation activity for all these compounds was initially evaluated in a screening with 25 $\mu$M each compound. BT10 was the only one that diminished the epimastigote growth by 50%, as previously mentioned. Although BT3 did not pass these criteria, it was the second best in terms of potency. Thus, BT10 and BT3 were used for some

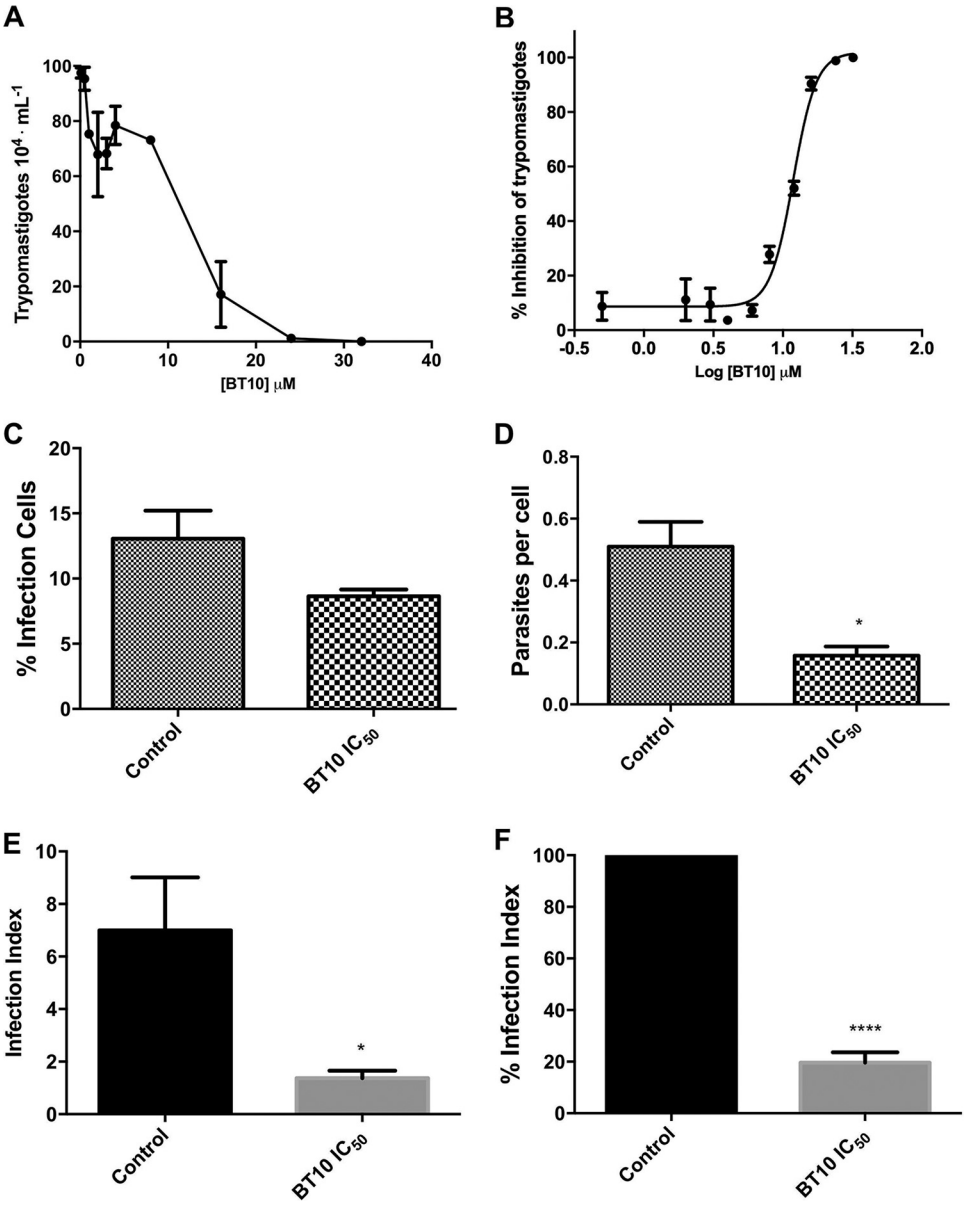


**FIG 7** Effect of BT10 on intracellular cycle and amastigote replication of *T. cruzi*. The effect of BT10 after infection on CHO-$K_1$ cells with trypomastigote forms was evaluated by counting the released parasites in a Neubauer chamber at the fifth day postinfection (A) and the corresponding concentration-response curve was plotted [$IC_{50(Tryp)} = 8.5 \pm 2.9\ \mu M$] (B). The percentage of infected cells (C) and the number of intracellular amastigotes per cell (D) were counted as described in Materials and Methods. The effect on amastigote replication was measured using the infection index (% of infected cells × number of parasites per cell) of treated parasites with $IC_{50}$ compared to the control (E) and the percentage of the infected index of treated parasites with $IC_{50}$ compared to the control (F). The values were plotted as the means ± SEM and compared to the control using a *t* test. *, $P < 0.05$; ****, $P < 0.0001$ (to establish significant differences). Panels A and B show a representative curve from three independent experiments. Panels C, D, E, and F correspond to three independent biological experiments.

experiments that allowed us to infer some structure-activity relationships. Both compounds contain a trifluoromethyl group (-$CF_3$) in the $R^1$ position of the benzothiazole moiety. Additionally, BT3 has a carboxyl group (-COOH) on $R^3$ of the phenyl moiety, while BT10 contains a methoxy group (-$OCH_3$) on $R^2$ and a hydroxyl group (-OH) on $R^3$. These data suggest that the inclusion of a fluorinated group on 2-phenylbenzothiazole derivatives contributes significantly to the antiproliferation activity. All these inferences are supported by the fact that benzothiazole derivatives such

as (*S*)-2-(3,4-difluorophenyl)-5-(3-fluoro-*N*-pyrrolidylamido) benzothiazole possess anti-*Trypanosoma brucei* activities (15). BT2 and BT6 compounds are closely related to BT3 and BT10, respectively, with the only difference being the absence of the -$CF_3$ substituent. The relevance of the fluorinated group in BT2 and BT6 could explain their lack of anti-*T. cruzi* activity (Fig. 1A to C). In fact, this finding is not surprising, since it is well known that fluorine atoms confer a set of physicochemical properties to organic compounds. Among them, it is worth mentioning improvement of lipophilicity, increased velocity of diffusion through biological membranes (32), an improved affinity for receptors (by favoring electrostatic interactions), and an increased binding affinity to active sites (7). In addition, the presence of fluorinated groups can also modify the acidity or basicity of the molecules, affecting the processes of absorption, metabolism, and bioavailability (33). To analyze the correlation of the activity of BT1 to BT14 to *in silico* drug-likeness analysis (rule of five [RO5]) (34), we determined whether the compounds in the collection follow these rules. Regarding the quantitative parameters of the RO5, we calculated the lipophilicity (expressed as the partition coefficient, log*P*) and topological polar surface area (TPSA; defined as the integration of the surfaces of polar atoms [in this case oxygen, nitrogen, and attached hydrogen]) (35). The computed parameters showed that BT3 and BT10 have log*P* values of 3.83 and 3.92 and TPSA values of 78.43 and 70.59, respectively. The presence of the -$CF_3$ group affected the predicted lipophilicity (comparing BT2 with BT3 and BT6 with BT10), resulting in intermediate log*P* values for the most active compounds. However, BT3 and BT10 were among those presenting the highest TPSA values in the collection. The increased TPSA values are probably due to the -COOH, -OH, and -$OCH_3$ groups on the phenyl moiety, which trigger electron withdrawal in combination with the -CF3 group in the case of BT10 and BT3. This fact could have a positive effect on antiproliferation activity. As the drug-likeness depends on both values, we propose here a parameter consisting of the product between log*P* and TPSA (see Table S1 in the supplemental material), which showed for our compounds a good prediction capacity in relation to their *in vitro* activity.

Among the drugs analyzed in our collection, BT10 was the only one that passed our criteria for being selected as an anti-*T. cruzi* drug for further studies, resulting in 2-fold more potent activity than that of BT3. Despite its antiproliferation effect, we could not detect signals of cell death in BT10-treated parasites, such as exposure of phosphatidylserine or loss of cytoplasmic membrane integrity. Thus, we hypothesized that BT10 would act as a trypanostatic compound rather than a trypanocide. Despite having a lower activity, we observed the same profile for BT3-treated parasites (Fig. S3), indicating that the mode of action of these structurally related compounds in *T. cruzi* is other than cytotoxicity, as previously reported for other benzothiazoles when evaluated on different cancer cell lines (36, 37). To obtain more clues about the inhibitory activity of BT10, we explored other parameters related to the maintenance of cell viability: the status of the mitochondrial inner membrane potential ($\Delta\Psi_m$), intracellular $Ca^{2+}$ levels, and endogenous production of ROS (26, 28). Our results show that a fraction of the BT10-treated cells had a diminished $\Delta\Psi_m$ with respect to that of the controls. This result indicates that their mitochondria are at least partially depolarized, which is consistent with the observed increase in intracellular $Ca^{2+}$ concentration.

Altogether, our results agree in part with the effects reported for benzothiazoles with antimicrobial activity in both Gram-positive and Gram-negative bacteria, although the effects are observed with 4-fold the MIC (between 3.91 and 15.6 $\mu$g/ml) (29). Notably, these effects by themselves point to a trypanostatic rather than trypanocidal activity. This possibility was confirmed by the fact that the effect of BT10 was reversible and produced alterations in the epimastigote cell cycle. Indeed, BT10 triggered a decrease of parasites in $G_0/G_1$ phases and an accumulation in the G/M phase at a concentration of 100 $\mu$M.

An alteration of the cell cycle consisting of the accumulation of parasites in the G/M phase could be a hallmark for DNA damage (31, 38). Our results revealed that BT10- and

**TABLE 1** Activity of BT3 and BT10 on different aspects of *T. cruzi* biology

| Parameter[a] | Value for: BT10 | BT3 |
|---|---|---|
| Epi $IC_{50}$ ($\mu$M), 28°C | 23.1 ± 1.75 | 48.8 ± 5.77 |
| $CC_{50}$ ($\mu$M) | 95.3 ± 3.3 | 127.6 ± 0.9 |
| Tryp $IC_{50}$ ($\mu$M) | 8.5 ± 2.9 | ND[b] |
| SI | | |
| $CC_{50}/IC_{50(Epi),\ 28°C}$ | 4.13 | 2.61 |
| $CC_{50}/IC_{50(Tryp)}$ | 11.21 | ND |
| Infection index inhibition (%) | 81.3 | ND |
| Loss of cytoplasmic membrane integrity | No | No |
| Induces ROS | No | ND |
| Alters intracellular $Ca^{2+}$ | No | ND |
| Affects parasite cell cycle | Yes | ND |
| Reversible effect in Epi | Yes | ND |
| kDNA damage | Yes | Yes |
| Affects amastigote replication | Yes | ND |
| Affects host cell infection | Yes | ND |

[a]Epi, epimastigote; Tryp, trypomastigote.
[b]ND, not determined.

BT3-treated cells (Fig. S4) had selectively damaged kDNA, raising three possibilities: (i) kDNA has a higher sensitivity to damage than gDNA; (ii) the mitochondrial DNA repair machinery (in the presence of the drug) is less efficient than that of the nuclear DNA; or (iii) the drug accumulates at higher concentrations in the mitochondria, submitting kDNA to higher concentrations of the drug than those for gDNA. Of course, a combination of the three possibilities cannot be ruled out. In any case, the mechanism by which damage occurs to kDNA remains elusive; it is possible that BT10 and BT3 will inhibit some DNA-dependent enzyme or inhibitor directly by inhibition of transcription and replication enzymes through direct interaction with DNA, as suggested by the helically arranged relationship of BT6 in crystal formation (39). This work supports the fact that the kDNA seems to be the main target to explain the anti-*T. cruzi* effect of BT3 and BT10. Indeed, the concentrations required to inhibit the triosephosphate isomerase are higher than those required to kill trypanosomatids (14, 15, 23). These data break the paradigm that the trypanocidal effect of benzothiazoles is due to the inhibition of triosephosphate isomerase, as traditionally proposed (13, 24, 25).

Regardless of the mechanism of action, the anti-*T. cruzi* activity on the parasite stages that are relevant for mammalian infection is a *sine qua non* condition for any compound to be proposed as a drug for the development of a treatment against Chagas disease. Remarkably, the treatment of infected cells with 8.5 $\mu$M BT10 caused a significant reduction in the number of intracellular amastigotes, in the trypomastigote burst, and in the infection index. These results, together with the drug selectivity (SI of 11.21) (Table 1), are particularly promising for the development of chemotherapy against the chronic phase of the disease.

To conclude, BT10 is a remarkable fluorinated hit compound for the development of new and better anti-*T. cruzi* compounds, which would be in accordance with the initiative proposed by the Drugs for Neglected Diseases initiative (DNDi) (40). Because the kinetoplast is the preferred target for BT10, other compounds based on its structure could have potential therapeutic applications for other diseases caused by kinetoplastid parasites, such as *Leishmania* spp. and *T. brucei*.

## MATERIALS AND METHODS

**Reagents.** All chemicals, reagents, and solvents for synthesis and MTT (methylthiazolyldiphenyltetrazolium bromide) were purchased from Sigma-Aldrich (St. Louis, MO, USA); Fluo-4 AM and annexin V-FITC were purchased from Invitrogen (Eugene, OR, USA); and culture media and fetal calf serum (FCS) were purchased from Cultilab (Campinas, Sao Paolo, Brazil).

**Synthesis of drugs and chemical characterization.** The 2-phenylbenzothiazole derivatives were synthesized by the following reaction conditions, which were previously described (14). Briefly, the appropriate 2-aminothiophenol (1.98 mmol) and substituted benzaldehyde (2.1 mmol) were reacted with an equimolar amount of $Na_2S_2O_5$ (2.1 mmol). The mixture was stirred with refluxing in dimethyl sulfoxide (DMSO) at ~120°C for 40 to 60 min. The product was precipitated by adding cool water and collected by vacuum filtration. The filtrate was then washed with an excess of water and left to dry. The remaining traces of sodium metabisulfite were extracted with brine and $CH_2Cl_2$, and the solvent was removed under vacuum. Finally, the resulting product was purified and recrystallized in ethanol-water (1:3). The progress of the reaction was monitored by thin-layer chromatography (TLC) analysis using a mix of ethyl acetate-hexane (1:1) as the eluent. All synthesized products were chemically characterized by $^1$H, $^{13}$C nuclear magnetic resonance (NMR) spectra on a Jeol GSX-300 spectrometer ($^1$H 300 MHz, $^{13}$C 75 MHz) or a Bruker-400 ($^1$H 400 MHz, $^{13}$C 101 MHz) or Bruker-750 ($^1$H 750 MHz, $^{13}$C 189 MHz) biospin (Bruker, Rheinstetten, Germany) using DMSO-$d_6$ and $CDCl_3$ as the solvent and trimethylsilyl as the internal reference. Chemical shift values ($\delta_{ax}$) are presented in parts per million (ppm), and coupling constants ($J$ values) are presented in Hertz (Hz). ESI-MS spectra were recorded on a Bruker micrOTOF-Q II. The uncorrected melting points were obtained in open-ended capillary tubes in Electrothermal 9300 digital equipment.

**(i) BT1 (2-phenyl-1,3-benzothiazole).** White needles, 77% yield, mp 95 to 96°C; $^1$H NMR (400 MHz, $CDCl_3$) $\delta$ 8.08 (m, 3H), 7.89 (dd, 1H, $^3J$ = 8 Hz, $^4J$ = 0.8 Hz), 7.5 (t, 1H, $J$ = 1.2 Hz), 7.48 (m, 3H), 7.37 (td, 1H, $^3J$ = 1.2 Hz); $^{13}$C NMR (101 MHz, $CDCl_3$) $\delta$ 168.0, 154.1, 135.1, 133.6, 130.9, 129.0 (2C), 127.5 (2C), 126.3, 125.1, 123.2, 121.6; MS(ESI) $C_{13}H_9NS$, $[M+H]^+$, *m/z* calculated 212.0528, found 212.0520.

**(ii) BT2 [4-(1,3-benzothiazol-2-yl)benzoic acid].** White powder, 63% yield, mp 332°C; $^1$H NMR (400 MHz, DMSO-$d_6$) $\delta$ 8.20 (d, 2H, $^3J$ = 8.4 Hz), 8.17 (s, 1H), 8.12 (d, 3H, $^3J$ = 8.0 Hz), 7.58 (t, 1H, $^3J$ = 7.6 Hz), 7.50 (t, 1H, $^3J$ = 7.6 Hz); $^{13}$C NMR (101 MHz, DMSO-$d_6$) $\delta$ 167.1, 166.6, 154.0, 136.8, 135.2, 133.7, 130.7 (2C), 127.7 (2C), 127.3, 126.4, 123.6, 122.9; MS(ESI) $C_{14}H_9NO_2S$, $[M+H]^+$, *m/z* calculated 256.0426, found 256.0394.

**(iii) BT3 (4-[5-(trifluoromethyl)-1,3-benzothiazol-2-yl]benzoic acid).** White needles, 82% yield, mp 257°C; $^1$H NMR (300 MHz, DMSO-$d_6$) $\delta$ 13.2 (s, 1H), 8.36 (d, 1H, $^3J$ = 6.6 Hz), 8.15 (d, 2H, $^3J$ = 8.4 Hz), 8.06 (d, 2H, $^3J$ = 8.7 Hz), 7.73 (dd, 1H, $^3J$ = 8.7, $^4J$ = 1.5 Hz); $^{13}$C NMR (75 MHz, DMSO-$d_6$) $\delta$ 169.2, 166.9, 153.4, 139.2, 136.1, 133.8, 130.7 (2C), 128.3, 127.9 (2C), 124.4, 122.2, 120.3; MS(ESI) $C_{15}H_8F_3NO_2S$, $[M+H]^-$, *m/z* calculated 322.0144, found 322.0226.

**(iv) BT4 [2-phenyl-5-(trifluoromethyl)-1,3-benzothiazole].** Yellow scaly crystals, 53% yield, mp 127 to 129°C; $^1$NMR (400 MHz, $CDCl_3$) $\delta$ 8.33 (t, 1H, $J$ = 0.8 Hz), 8.09 (m, 2H), 8.0 (dt, 1H, $^3J$ = 8.6 Hz, $^4J$ = 0.4 Hz), 7.52 (m, 3 H); $^{13}$C NMR (101 MHz, $CDCl_3$) $\delta$ 170.1, 153.7, 138.4, 133.0, 131.5, 129.1 (2C), 127.7 (2C), 125.5, 122.2, 121.5, 120.4; MS(ESI) $C_{14}H_8F_3NS$, $[M+H]^+$, *m/z* calculated 280.0402, found 280.0379.

**(v) BT5 (methyl 4-[5-(trifluoromethyl)-1,3-benzothiazol-2-yl]-benzoate).** White needles, 41% yield, mp 242°C; $^1$H NMR (300 MHz, DMSO-$d_6$) $\delta$ 8.43 (s, 1H), 8.41 (s, 1H), 8.21 (d, 2H, $^3J$ = 11.2 Hz), 8.09 (d, 2H, $^3J$ = 11.2 Hz), 7.78 (d, 1H, $^3J$ = 11.2 Hz), 3.87 (s, 3H); $^{13}$C NMR (75 MHz, DMSO-$d_6$) $\delta$ 169.1, 165.9, 153.6, 139.3, 136.7, 132.8, 130.5 (2C), 128.6, 128.1 (2C), 124.3, 122.3, 120.4, 52.7; MS(ESI) $C_{16}H_{10}F_3NO_2S$, $[M+H]^+$, *m/z* calculated 338.0457, found 338.0452.

**(vi) BT6 [2-(4-hydroxy-3-methoxyphenyl)-benzothiazole].** Gray powder, 87% yield, mp 162 to 163°C; $^1$H NMR (300 MHz, DMSO-$d_6$) $\delta$ 9.85 (s, 1H), 8.03 (d, 1H, $^3J$ = 8.25 Hz), 7.97 (d, 1H, $^3J$ = 8.4 ppm), 7.61 (d, 1H, $^4J$ = 2.1 Hz), 7.47 (dd, 1H, $^3J$ = 8.1 Hz, $^4J$ = 2.1 Hz), 7.47 (m, 1H), 7.37 (td, 1H, $J$ = 7.6 Hz), 6.91 (d, 1H, $J$ = 8.1 Hz), 3.87 (s, 3H); $^{13}$C NMR (75 MHz, DMSO-$d_6$) $\delta$ 167.9, 154.0, 150.4, 148.5, 134.6, 126.8, 125.3, 124.7, 122.7, 122.5, 121.7, 116.3, 110.4, 56.1; MS(ESI) $C_{14}H_{11}NO_2S$, $[M+H]^+$, *m/z* calculated 258.0583, found 258.0583.

**(vii) BT7 [3-(1,3-benzothiazol-2-yl)-benzoic acid].** Gray crystals, 77% yield, mp 257°C; $^1$H NMR (750 MHz, DMSO-$d_6$) $\delta$ 13.40 (s, 1H), 8.63 (s, 1H), 8.31 (d, 1H, $^3J$ = 4.4 Hz), 8.18 (d, 1H, $^3J$ = 4 Hz), 8.12 (d, 1H, $^3J$ = 4.4 Hz), 8.1 (d, 1H, $^3J$ = 4.4 Hz), 7.72 (t, 1H, $^3J$ = 4), 7.57 (t, 1H, $^3J$ = 4), 7.49 (t, 1H, $^3J$ = 3.8 Hz); $^{13}$C NMR (189 MHz, DMSO-$d_6$) $\delta$ 167.0, 166.7, 153.9, 134.9, 133.6, 132.3, 131.7, 130.4, 128, 127.3, 126.3, 123.5, 122.9; MS(ESI) $C_{14}H_9NO_2S$, $[M+H]^+$, *m/z* calculated 256.0426, found 256.0407.

**(viii) BT8 [methyl 4-(1,3-benzothiazol-2-yl)-benzoate].** Solid brown, 67% yield, mp 158°C; $^1$H NMR (400 MHz, DMSO-$d_6$) $\delta$ 8.25 (d, 2H, $^3J$ = 8.8 Hz), 8.21 (dd, 1H, $J$ = 1), 8.14 (d, 2H, $^3J$ = 8.8 Hz), 7.6 (td, 1H, $^3J$ = 7.6 Hz, $^4J$ = 1.2 Hz), 7.52 (td, 1H, $^3J$ = 7.7 Hz, $^4J$ = 1.2 Hz), 3.91 (s, 3H); $^{13}$C NMR (101 MHz, DMSO-$d_6$) $\delta$ 166.4, 166.0, 153.9, 137.2, 135.2, 132.1, 130.6 (2C), 127.9 (2C), 127.4, 126.5, 123.7, 123.0, 52.8; MS(ESI) $C_{15}H_{11}NO_2S$, $[M+H]^+$, *m/z* calculated 270.0583, found 270.0563.

**(ix) BT9 [methyl 3-(1,3-benzothiazol-2-yl)-benzoate].** White powder, 87% yield, mp 248°C; $^1$H NMR (750 MHz, DMSO-$d_6$) $\delta$ 8.62 (s, 1H), 8.32 (d,1H $^3J$ = 8.25 Hz,), 8.17 (d, 1H, $^3J$ = 7.5 Hz,), 8.11 (t, 2H, $^3J$ = 8.25 Hz), 7.73 (t, 1H, $^3J$ = 7.5 Hz,), 7.57 (t, 1H, $^3J$ = 7.87 Hz), 7.49 (t, 1H, $^3J$ = 7.87 Hz), 3.92 (s, 3H); $^{13}$C NMR (189 MHz, DMSO-$d_6$) $\delta$ 166.5, 166, 153.9, 134.9, 133.7, 132.2, 132.0, 131.1, 130.6, 127.6, 127.3, 126.3, 123.5, 122.9, 52.9; MS(ESI) $C_{15}H_{11}NO_2S$, $[M+H]^+$, *m/z* calculated 270.0583, found 270.0575.

**(x) BT10 (2-methoxy-4-[5-(trifluoromethyl)-1,3-benzothiazol-2-yl]phenol).** Brownish crystalline powder, 22% yield, mp 137°C; $^1$H NMR (300 MHz, DMSO-$d_6$) 8.3 (d, 1H, $^3J$ = 6 Hz), 8.28 (s, 1H), 7.68 (dd, 1H, $^3J$ = 9 Hz, $^4J$ = 3 Hz), 7.6 (d, 1H, $^3J$ = 3 Hz), 7.51 (dd, 1H, $^3J$ = 8.4 Hz, $^4J$ = 2.1 Hz), 6.94 (d, 1H, $^3J$ = 8.1Hz), 3.87 (s, 3H); $^{13}$C NMR (75 MHz, DMSO-$d_6$) $\delta$ 170.6, 153.7, 151.0, 148.5, 138.8, 128, 124.1, 123.9, 122.1, 121.3, 119.3, 116.4, 110.6, 56.1; MS(ESI) $C_{15}H_{10}F_3NO_2S$, $[M+H]^+$, *m/z* calculated 326.0457, found 326.0429.

**(xi) BT11 [4-(1,3-benzothiazol-2-yl)-2,6-dimethoxyphenol].** Gray crystals, 85% yield, mp 135°C; $^1$H NMR (750 MHz, $CDCl_3$) $\delta$ 8.03 (d, 1H, $^3J$ = 8.25 Hz), 7.87 (d, 1H, $^3J$ = 7.5 Hz), 7.47 (m, 1H), 7.35 (td, 1H, $^3J$ = 7.5 Hz), 7.34 (s, 2H), 3.99 (s, 6× H); $^{13}$C NMR (189 MHz, $CDCl_3$) $\delta$ 168.1, 154.0, 147.3 (2C), 137.7, 134.8,

126.3, 125.1, 124.9, 122.8, 121.5, 104.5 (2C), 56.5 (2C); MS(ESI) $C_{15}H_{13}NO_3S$, $[M+H]^+$, *m/z* calculated 288.0689, found 288.0695.

**(xii) BT12 [4-(1,3-benzothiazol-2-yl)benzonitrile].** White crystalline powder, 88% yield, mp 158°C; $^1$H NMR (300 MHz, DMSO-$d_6$) $\delta$ 8.21 (d, 2H, $J = 8.4$ Hz), 8.16 (d, 1H, $J = 8.1$ Hz), 8.08 (d, 1H, $J = 8.07$ Hz), 7.98 (d, 2H, $J = 8.4$ Hz), 7.56 (m, 1H), 7.49 (t, 1H, $J = 7.5$ Hz); $^{13}$C NMR (75 MHz, DMSO-$d_6$) $\delta$ 165.7, 153.8, 137.0, 135.3, 133.7 (2C), 128.2 (2C), 127.4, 126.6, 123.8, 123.0, 118.7, 113.7; MS(ESI) $C_{14}H_8N_2S$, $[M+H]^+$, *m/z* calculated 237.0481, found 237.0482.

**(xiii) BT13 [2-(4-chlorophenyl)-1,3-benzothiazole].** Gray crystals, 72% yield, mp 105°C; $^1$H NMR (750 MHz, $CDCl_3$) $\delta$ 8.06 (d, 1H, $^3J = 8.2$ Hz), 8.02 (d, 2H, $^3J = 9$ Hz, $^4J = 2.25$ Hz), 7.9 (d, 1H, $^3J = 8.2$ Hz), 7.5 (t, 1H, $^3J = 7.5$ Hz), 7.46 (d, 2H, $^3J = 9$ Hz, $^4J = 2.25$ Hz), 7.39 (td, 1H, $J = 7.12$ Hz); $^{13}$C NMR (189 MHz, $CDCl_3$) $\delta$ 166.6, 154.0, 137.0, 135.0, 132.1, 129.2 (2C), 128.7 (2C), 126.4, 125.4, 123.2, 121.6; MS(ESI) $C_{13}H_8NSCl$, $[M+H]^+$, *m/z* calculated 246.0139, found 246.0134.

**(xiv) BT14 [2-(4-bromophenyl)-1,3-benzothiazole].** Yellow crystals, 38% yield, mp 124°C; $^1$H NMR (750 MHz, $CDCl_3$) $\delta$ 8.06 (d, 1H, $^3J = 8.2$ Hz), 7.95 (d, 2H, $^3J = 8$ Hz), 7.89 (d, 1H, $^3J = 8.2$ Hz), 7.62 (d, 2H, $^3J = 8.2$ Hz), 7.49 (t, 1H, $^3J = 7.5$ Hz), 7.39 (td, 1H, $^3J = 7.5$ Hz); $^{13}$C NMR (189 MHz, $CDCl_3$) $\delta$ 166.6, 154.0, 135.0, 132.5, 132.2 (2C), 128.9 (2C), 126.5, 125.4, 123.3, 121.6; MS(ESI) $C_{13}H_8NSBr$, $[M+H]^+$, *m/z* calculated 289.9634, found 289.9613.

**Cells and parasite cultures.** *T. cruzi* epimastigotes (CL strain clone 14) were maintained in the exponential growth phase by subculturing every 48 h in LIT medium at 28°C (41). The Chinese hamster ovary cell line (CHO-$K_1$) was cultivated in RPMI 1640 medium supplemented with 10% heat-inactivated FCS, 0.15% (wt/vol) $NaHCO_3$, 100 U/ml penicillin, and 100 mg/ml streptomycin at 37°C in a humidified atmosphere containing 5% $CO_2$. Trypomastigotes were obtained by infection in CHO-$K_1$ cells with trypomastigotes at 37°C in the presence of 10% FCS. After 24 h, the cells were maintained at 33°C and 2% FCS (42). Trypomastigotes were collected from the extracellular medium 5 days after infection.

***In vitro* inhibition of proliferation assays.** The cell density of exponentially proliferating epimastigotes (approximately $50 \times 10^6$ parasites/ml) was adjusted to $2.5 \times 10^6$ cells/ml and transferred (200 $\mu$l/well) into 96-well plates (43). Epimastigote proliferation was measured by reading the optical density (OD) at 620 nm every 24 h through the exponential and stationary phases (9 days). The OD values were converted to cell density values (cells per milliliter) by using a calibration curve obtained by measuring the OD values at 620 nm of parasite suspensions at different known densities. The concentrations of the compound that inhibited 50% of epimastigote proliferation ($IC_{50}$) were determined in the exponential growth phase (5th day) by fitting the cell density data to a sigmoidal concentration-response curve using GraphPad Prism v.6. A combination of 60 $\mu$M rotenone and 0.5 $\mu$M antimycin A (RA) was used as a positive control for proliferation inhibition. Untreated parasites supplemented with DMSO (the vehicle for the drugs) and unsupplemented parasites were used as negative controls. The compounds were evaluated in quadruplicate in each experiment, and the results correspond to three independent experiments.

**The effect of BT3 and BT10 compounds on mammalian cell viability.** CHO-$K_1$ cells ($1 \times 10^5$ cells/well) in 100 $\mu$l of RPMI medium supplemented with FCS (10%) were seeded in 96-well plates with or without (control) different concentrations of the most active compounds, BT3 (16 to 800 $\mu$M) and BT10 (8 to 288 $\mu$M). Cell viability was determined by the MTT assay as previously described (44). The produced formazan was solubilized in 50 $\mu$l of DMSO, and the OD was measured at 540 nm using 690 nm as a reference. The $IC_{50}$ was determined by fitting the data to a sigmoidal dose-response curve using GraphPad Prism v.6. Each assay was developed in quadruplicate, and the results correspond to the means from three independent experiments.

**Analysis of phosphatidylserine exposure, $\Delta\Psi_m$ depolarization, intracellular $Ca^{2+}$ levels, and hydrogen peroxide production.** Epimastigotes ($2.5 \times 10^6$ cell/ml) were incubated for 5 days, unless otherwise stated, in the presence or absence (control) of 25 $\mu$M and 50 $\mu$M BT10 (approximately 1× and 2× the $IC_{50}$, respectively). To determine phosphatidylserine exposure, the cells were labeled with propidium iodide (PI) and annexin V-FITC (Molecular Probes) according to the manufacturer's instructions. As positive controls for cytoplasmic membrane permeabilization and extracellular exposure of phosphatidylserine, the parasites were treated with 150 $\mu$M digitonin or 1 $\mu$M staurosporine for 30 min, respectively (45). For determining variations in $\Delta\Psi_m$, cells were aliquoted in fractions at densities of $1.0 \times 10^6$ cells/ml. Half of the aliquot was incubated for 15 min with 1 $\mu$M FCCP in phosphate-buffered saline (PBS), while the other half was left untreated. All samples then were centrifuged for 10 min at $2{,}700 \times g$ and resuspended in HEPES-glucose buffer (50 mM HEPES [pH 7.4], 116 mM NaCl, 5.4 mM KCl, 0.8 mM $MgSO_4$, 5.5 mM glucose, and 2 mM $CaCl_2$). The cells were labeled by the addition of 256 nM rhodamine 123 (Rh123) for 20 min at 28°C (46). To analyze variations in the intracellular $Ca^{2+}$ levels, the parasites were incubated with 5 mM Fluo-4 AM (Invitrogen) for 1 h at 28°C. After this period, the cells were washed twice with HEPES-glucose and resuspended in the same buffer (47). To evaluate the production of hydrogen peroxide, the parasites treated with 1× $IC_{50}$ or 2× $IC_{50}$ of BT10 for 24 h were incubated for 30 min at 28°C in HEPES-glucose buffer in the presence of 10 $\mu$M carboxy-DCFDA. In all cases, the cells were analyzed by flow cytometry on a Guava cytometer (General Electric), with 10,000 events collected, and analyzed using FlowJo software (v10.1r7).

**DNA content and cell cycle analysis.** Parasites ($2.5 \times 10^6$ cells/ml) treated with 25 and 100 $\mu$M BT10 (or left untreated as a negative control) for 5 days were collected by centrifugation ($2{,}700 \times g$ for 5 min), washed in PBS, fixed in 70% ethanol for 12 h, and incubated with 10 $\mu$g/ml RNase A (Thermo Scientific) for 30 min at 37°C. To measure the DNA content, parasite cells were stained with 40 $\mu$g/ml propidium iodide (Molecular Probes/Invitrogen) and analyzed by flow cytometry on an acoustic focusing cytometer

(Attune; Applied Biosystems), with 50,000 events collected (31). Histograms (number of counts by the detector BL2 per area unit), scatter plots (side scatter [SSC] area by forward scatter [FSC] area), and gates for each cell cycle phase were analyzed using FlowJo software (v10.1r7). Cell cycle data were fitted using the Dean-Jett Fox (DJF) model included in the FlowJo software.

**Analysis of DNA damage by TUNEL assay.** Epimastigotes treated with 25 $\mu$M BT10 (or left untreated as a control) in the exponential growth phase were collected by centrifugation, washed with PBS, and fixed by incubation with 4% paraformaldehyde for 10 min at room temperature. After washing and resuspension in PBS, the cells were permeabilized by treatment with 0.1% Triton X-100 for 10 min at 26°C and were treated with 0.1 M glycine for 5 min to neutralize the remaining aldehyde groups. The TUNEL assay was performed by using the DeadEnd fluorometric TUNEL system kit (G3250; Promega) according to the manufacturer's protocol. VECTASHIELD mounting medium with 4′,6-diamidino-2-phenylindole (DAPI) (Vector Labs) was added to be used as an antifade mounting solution and to stain nuclear and kinetoplast DNA. For each group analyzed, we analyzed at least 100 cells in at least three different image fields. This assay was carried out in triplicate. To confirm these results, we analyzed an aliquot of the cells under each condition by cytometry. Histograms (counts by BL1 area), scatter plots (SSC area by FSC area), and gates to exclude cell debris/doublets were performed using Attune Cytometric software (v.1.2.5) and FlowJo software (v10.1r7). In total, 10,000 events were analyzed for each sample.

**Effect of BT10 on amastigote replication and trypomastigote release.** CHO-$K_1$ cells ($5.0 \times 10^4$ per well) were maintained in 24-well plates in RPMI medium supplemented with 10% FCS at 37°C. To perform the infections, the cells were incubated with trypomastigote forms ($2.5 \times 10^6$ per well) for 4 h. After this period, parasites in the supernatant were removed by washing the plates twice with PBS, and the cells were incubated overnight in RPMI medium supplemented with 10% FCS at 37°C in the presence of different concentrations of BT10 or left untreated (control). The plates were then incubated at 33°C to allow the parasite to complete the infection cycle, as previously reported (43). To measure the effect on amastigote replication, after 48 h, the CHO-$K_1$ cells and parasites were fixed with 4% paraformaldehyde, and nuclei were stained with Hoechst 33342 (Invitrogen) for counting. We acquired fluorescence microscopy images corresponding to 30 fields per biological sample at a magnification of ×200 (EVOS FL cell imaging system; Thermo Fisher Scientific). Cells, parasites, and infected cells were counted using ImageJ software. The infection index was calculated as the arithmetical product of the percentage of infected cells and the number of parasites per cell. The effect of BT10 on trypomastigote production was determined by collecting samples of the extracellular medium on the fifth day postinfection and counting the number of trypomastigotes in a Neubauer chamber (38). The results correspond to the means from three independent experiments, each performed in triplicate.

**Data treatment and statistical analysis.** Curve adjustments, regressions, and statistical analyses were performed with the GraphPad Prism 7 analysis tools. All assays were performed at least in biological triplicates. The specific details of the statistical analysis for each experiment are described in the corresponding figure legend. In general, the Student's *t* test was used to analyze differences between the two groups. *P* values of less than 0.05 were considered statistically significant.

## SUPPLEMENTAL MATERIAL

Supplemental material is available online only.

**SUPPLEMENTAL FILE 1**, PDF file, 1 MB.

## ACKNOWLEDGMENTS

This work was supported by Fundação de Amparo à Pesquisa do Estado de São Paulo grant 2016/06034-2 (awarded to A.M.S.) (www.fapesp.br), Conselho Nacional de Desenvolvimento Científico e Tecnológico (CNPq) grants 301971/2017-0 and 404769/2018-7 (awarded to A.M.S.) (www.cnpq.br), and Research Council United Kingdom Global Challenges Research Fund under grant agreement "A Global Network for Neglected Tropical Diseases" (grant MR/P027989/1) (awarded to A.M.S.) (https://www.ukri.org). Further funding was from Consejo Nacional de Ciencia y Tecnología (CONACyT), grant 2011-1 no. 168116 (awarded to J.G.T.-F.); Secretaria de Investigación y Posgrado del Instituto Politécnico Nacional (SIP-IPN) grants 20120151, 20130488, 20140109, 20150309, and 20160126 (awarded to J.G.T.-F.); and Red Macrouniversidades and CONACyT (student grants CRA/027-28/2016 and 246663).

We thank Alexandre Moura for technical assistance during this work.

R.I.C.-H., J.G.T.-F., and S.M.-C. synthesized and characterized compounds. R.G., R.I.C.-H., and A.M.S. conceived and designed the biological experiments. R.I.C.-H., R.G., M.C., A.M.S., and M.S.S. performed the experiments. R.I.C.-H., R.G., A.M.S., and M.C.E. analyzed the data. J.G.T.-F. and A.M.S. contributed reagents/materials/analysis tools. R.I.C.-H., A.M.S., and R.G. wrote the paper. All authors gave approval to the final version of the paper.

## REFERENCES


1. World Health Organization. 2018. Chagas disease (American trypanosomiasis). World Health Organization, Geneva, Switzerland.
2. Bonney KM. 2014. Chagas disease in the 21st century: a public health success or an emerging threat? Parasite 21:11. https://doi.org/10.1051/parasite/2014012.
3. Bern C. 2015. Chagas' disease. N Engl J Med 373:456–466. https://doi.org/10.1056/NEJMra1410150.
4. Liu Q, Zhou X-N. 2015. Preventing the transmission of American trypanosomiasis and its spread into non-endemic countries. Infect Dis Poverty 4:60. https://doi.org/10.1186/s40249-015-0092-7.
5. Brener Z. 1973. Biology of *Trypanosoma Cruzi*. Annu Rev Microbiol 27:347–382. https://doi.org/10.1146/annurev.mi.27.100173.002023.
6. Alves MJM, Colli W. 2007. *Trypanosoma cruzi*: adhesion to the host cell and intracellular survival. IUBMB Life 59:274–279. https://doi.org/10.1080/15216540701200084.
7. Purser S, Moore PR, Swallow S, Gouverneur V. 2008. Fluorine in medicinal chemistry. Chem Soc Rev 37:320–330. https://doi.org/10.1039/b610213c.
8. Boscardin SB, Torrecilhas ACT, Manarin R, Revelli S, Rey EG, Tonelli RR, Silber AM. 2010. Chagas' disease: an update on immune mechanisms and therapeutic strategies. J Cell Mol Med 14:1373–1384. https://doi.org/10.1111/j.1582-4934.2010.01007.x.
9. Rassi A, Rassi A, Marin-Neto JA. 2010. Chagas disease. Lancet 375:1388–1402. https://doi.org/10.1016/S0140-6736(10)60061-X.
10. Gouttefangeas C, Britten CM, Badalians ED, Pawelec G. 2007. CIMT meets strategies for immune therapy: Mainz, Germany, 04–05 May 2006. Cancer Immunol Immunother 56:397–402. https://doi.org/10.1007/s00262-006-0211-1.
11. Jensen RE, Englund PT. 2012. Network news: the replication of kinetoplast DNA. Annu Rev Microbiol 66:473–491. https://doi.org/10.1146/annurev-micro-092611-150057.
12. Duschak VG. 2016. Targets and patented drugs for chemotherapy of Chagas disease in the last 15 year period. Recent Pat Antiinfect Drug Discov 11:74–173. https://doi.org/10.2174/1574891X11666161024165304.
13. Téllez-Valencia A, Avila-Ríos S, Pérez-Montfort R, Rodríguez-Romero A, Tuena de Gómez-Puyou M, López-Calahorra F, Gómez-Puyou A. 2002. Highly specific inactivation of triosephosphate isomerase from *Trypanosoma cruzi*. Biochem Biophys Res Commun 295:958–963. https://doi.org/10.1016/s0006-291x(02)00796-9.
14. Cuevas-Hernández RI, Correa-Basurto J, Flores-Sandoval CA, Padilla-Martínez II, Nogueda-Torres B, Villa-Tanaca MDL, Tamay-Cach F, Nolasco-Fidencio JJ, Trujillo-Ferrara JG. 2016. Fluorine-containing benzothiazole as a novel trypanocidal agent: design, in silico study, synthesis and activity evaluation. Med Chem Res 25:211–224. https://doi.org/10.1007/s00044-015-1475-9.
15. Patrick DA, Gillespie JR, McQueen J, Hulverson MA, Ranade RM, Creason SA, Herbst ZM, Gelb MH, Buckner FS, Tidwell RR. 2017. Urea derivatives of 2-aryl-benzothiazol-5-amines: a new class of potential drugs for human African trypanosomiasis. J Med Chem 60:957–971. https://doi.org/10.1021/acs.jmedchem.6b01163.
16. Bae HJ, Lee YS, Kang DW, Koo JS, Yoon BW, Roh JK, Gu JS. 2000. Neuroprotective effect of low dose riluzole in gerbil model of transient global ischemia. Neurosci Lett 294:29–32. https://doi.org/10.1016/s0304-3940(00)01536-6.
17. Kumar P, Shrivastava B, Pandeya SN, Tripathi L, Stables JP. 2012. Design, synthesis, and anticonvulsant evaluation of some novel 1, 3 benzothiazol-2-yl hydrazones/acetohydrazones. Med Chem Res 21:2428–2442. https://doi.org/10.1007/s00044-011-9768-0.
18. Cressier D, Prouillac C, Hernandez P, Amourette C, Diserbo M, Lion C, Rima G. 2009. Synthesis, antioxidant properties and radioprotective effects of new benzothiazoles and thiadiazoles. Bioorg Med Chem 17:5275–5284. https://doi.org/10.1016/j.bmc.2009.05.039.
19. Ha YM, Park JY, Park YJ, Park D, Choi YJ, Kim JM, Lee EK, Han YK, Kim J-A, Lee JY, Moon HR, Chung HY. 2011. Synthesis and biological activity of hydroxy substituted phenyl-benzo[d]thiazole analogues for antityrosinase activity in B16 cells. Bioorg Med Chem Lett 21:2445–2449. https://doi.org/10.1016/j.bmcl.2011.02.064.
20. Mortimer CG, Wells G, Crochard J-P, Stone EL, Bradshaw TD, Stevens MFG, Westwell AD. 2006. Antitumor benzothiazoles. 26. 1 2–(3,4-Dimethoxyphenyl)-5-fluorobenzothiazole (GW 610, NSC 721648), a simple fluorinated 2-arylbenzothiazole, shows potent and selective inhibitory activity against lung, colon, and breast cancer cell lines. J Med Chem 49:179–185. https://doi.org/10.1021/jm050942k.
21. Hiyoshi H, Goto N, Tsuchiya M, Iida K, Nakajima Y, Hirata N, Kanda Y, Nagasawa K, Yanagisawa J. 2014. 2-(4-Hydroxy-3-methoxyphenyl)-benzothiazole suppresses tumor progression and metastatic potential of breast cancer cells by inducing ubiquitin ligase CHIP. Sci Rep 4:7095. https://doi.org/10.1038/srep07095.
22. Sahu PK, Sahu PK, Gupta SK, Thavaselvam D, Agarwal DD. 2012. Synthesis and evaluation of antimicrobial activity of 4H-pyrimido[2,1-b]benzothiazole, pyrazole and benzylidene derivatives of curcumin. Eur J Med Chem 54:366–378. https://doi.org/10.1016/j.ejmech.2012.05.020.
23. Delmas F, Avellaneda A, Di Giorgio C, Robin M, De Clercq E, Timon-David P, Galy J-P. 2004. Synthesis and antileishmanial activity of (1,3-benzothiazol-2-yl) amino-9-(10H)-acridinone derivatives. Eur J Med Chem 39:685–690. https://doi.org/10.1016/j.ejmech.2004.04.006.
24. Espinoza-Fonseca LM, Trujillo-Ferrara JG. 2006. Toward a rational design of selective multi-trypanosomatid inhibitors: a computational docking study. Bioorg Med Chem Lett 16:6288–6292. https://doi.org/10.1016/j.bmcl.2006.09.029.
25. Olivares-Illana V, Pérez-Montfort R, López-Calahorra F, Costas M, Rodríguez-Romero A, Tuena de Gómez-Puyou M, Gómez Puyou A. 2006. Structural differences in triosephosphate isomerase from different species and discovery of a multitrypanosomatid inhibitor. Biochemistry 45:2556–2560. https://doi.org/10.1021/bi0522293.
26. Smirlis D, Duszenko M, Ruiz A, Scoulica E, Bastien P, Fasel N, Soteriadou K. 2010. Targeting essential pathways in trypanosomatids gives insights into protozoan mechanisms of cell death. Parasit Vectors 3:107. https://doi.org/10.1186/1756-3305-3-107.
27. Smirlis D, Soteriadou K. 2011. Trypanosomatid apoptosis: "apoptosis" without the canonical regulators. Virulence 2:253–256. https://doi.org/10.4161/viru.2.3.16278.
28. Irigoín F, Inada NM, Fernandes MP, Piacenza L, Gadelha FR, Vercesi AE, Radi R. 2009. Mitochondrial calcium overload triggers complement-dependent superoxide-mediated programmed cell death in Trypanosoma cruzi. Biochem J 418:595–604. https://doi.org/10.1042/BJ20081981.
29. Selvarajah J, Elia A, Carroll VA, Moumen A. 2015. DNA damage-induced S and G2/M cell cycle arrest requires mTORC2-dependent regulation of Chk1. Oncotarget 6:427–440. https://doi.org/10.18632/oncotarget.2813.
30. Yin M, Guo B, Panadero A, Frank C, Wrzosek C, Slocum HK, Rustum YM. 1999. Cyclin E–Cdk2 activation is associated with cell cycle arrest and inhibition of DNA replication induced by the thymidylate synthase inhibitor tomudex. Exp Cell Res 247:189–199. https://doi.org/10.1006/excr.1998.4346.
31. Zuma AA, Mendes IC, Reignault LC, Elias MC, de Souza W, Machado CR, Motta M. 2014. How *Trypanosoma cruzi* handles cell cycle arrest promoted by camptothecin, a topoisomerase I inhibitor. Mol Biochem Parasitol 193:93–100. https://doi.org/10.1016/j.molbiopara.2014.02.001.
32. Smart BE. 2001. Fluorine substituent effects (on bioactivity). J Fluor Chem 109:3–11. https://doi.org/10.1016/S0022-1139(01)00375-X.
33. Swallow S. 2015. Fluorine in medicinal chemistry, p 65–133. *In* King FD, Lawton G (ed), Progress in medicinal chemistry, 1st ed. Elsevier B.V., Amsterdam, the Netherlands.
34. Lipinski CA, Lombardo F, Dominy BW, Feeney PJ. 2001. Experimental and computational approaches to estimate solubility and permeability in drug discovery and development settings. Adv Drug Deliv Rev 46:3–26. https://doi.org/10.1016/S0169-409X(00)00129-0.
35. Ertl P, Rohde B, Selzer P. 2000. Fast calculation of molecular polar surface area as a sum of fragment-based contributions and its application to the prediction of drug transport properties. J Med Chem 43:3714–3717. https://doi.org/10.1021/jm000942e.
36. Xuejiao S, Yong X, Ningyu W, Lidan Z, Xuanhong S, Youzhi X, Tinghong Y, Yaojie S, Yongxia Z, Luoting Y. 2013. A novel benzothiazole derivative YLT322 induces apoptosis via the mitochondrial apoptosis pathway *in vitro* with anti-tumor activity in solid malignancies. PLoS One 8:e63900. https://doi.org/10.1371/journal.pone.0063900.
37. Wang Z, Shi X-H, Wang J, Zhou T, Xu Y-Z, Huang T-T, Li Y-F, Zhao Y-L, Yang L, Yang S-Y, Yu L-T, Wei Y-Q. 2011. Synthesis, structure–activity relationships and preliminary antitumor evaluation of benzothiazole-2-thiol derivatives as novel apoptosis inducers. Bioorg Med Chem Lett 21:1097–1101. https://doi.org/10.1016/j.bmcl.2010.12.124.

38. Girard R, Crispim M, Stolić I, Damasceno FS, Santos da Silva M, Pral EMF, Elias MC, Bajić M, Silber AM. 2016. An aromatic diamidine that targets kinetoplast DNA, impairs the cell cycle in *Trypanosoma cruzi*, and diminishes trypomastigote release from infected mammalian host cells. Antimicrob Agents Chemother 60:5867–5877. https://doi.org/10.1128/AAC.01595-15.
39. Cuevas-Hernández R, Padilla-Martínez I, Martínez-Cerón S, Vásquez-Moctezuma I, Trujillo-Ferrara J. 2017. Helical arrangement of 2–(4-hydroxy-3-methoxyphenyl)-benzothiazole in crystal formation and biological evaluation on HeLa cells. Crystals 7:171. https://doi.org/10.3390/cryst7060171.
40. Don R, Ioset J-R. 2014. Screening strategies to identify new chemical diversity for drug development to treat kinetoplastid infections. Parasitology 141:140–146. https://doi.org/10.1017/S003118201300142X.
41. Brener Z, Chiari E. 1965. Aspects of early growth of different *Trypanosoma cruzi* strains in culture medium. J Parasitol 51:922–926. https://doi.org/10.2307/3275869.
42. Almeida-de-Faria M, Freymüller E, Colli W, Alves M. 1999. *Trypanosoma cruzi*: characterization of an intracellular epimastigote-like form. Exp Parasitol 92:163–274.
43. Magdaleno A, Ahn I-Y, Paes LS, Silber AM. 2009. Actions of a proline analogue, L-thiazolidine-4-carboxylic acid (T4C), on *Trypanosoma cruzi*. PLoS One 4:e4534. https://doi.org/10.1371/journal.pone.0004534.
44. Mosmann T. 1983. Rapid colorimetric assay for cellular growth and survival: application to proliferation and cytotoxicity assays. J Immunol Methods 65:55–63. https://doi.org/10.1016/0022-1759(83)90303-4.
45. Jimenez V, Paredes R, Sosa MA, Galanti N. 2008. Natural programmed cell death in *T. cruzi* epimastigotes maintained in axenic cultures. J Cell Biochem 105:688–698. https://doi.org/10.1002/jcb.21864.
46. Girard R, Crispim M, Alencar MB, Silber AM. 2018. Uptake of l-alanine and its distinct roles in the bioenergetics of *Trypanosoma cruzi*. mSphere 3:e00338-18. https://doi.org/10.1128/mSphereDirect.00338-18.
47. Dolai S, Yadav RK, Pal S, Adak S. 2009. Overexpression of mitochondrial *Leishmania major* ascorbate peroxidase enhances tolerance to oxidative stress-induced programmed cell death and protein damage. Eukaryot Cell 8:1721–1731. https://doi.org/10.1128/EC.00198-09.